Topographic control of ground motions and landslides from the 2015 Gorkha earthquake

Audrey M. Dunham[1], Eric Kiser[1], Jeffrey S. Kargel[2], Umesh K. Haritashya[3], C. Scott Watson[4], Dan H. Shugar[5], Amanda Hughes[1], Peter G. DeCelles[1]

[1]The University of Arizona, Tucson AZ, [2]Planetary Science Institute, Tucson AZ, [3]University of Dayton, Dayton, OH, [4]University of Leeds, Leeds, LS2 9JT, UK, [5]University of Calgary, Canada

MOTIVATION

Coseismic landslides are a major secondary hazard of large earthquakes, particularly in high mountainous regions like the Himalaya. Studying where and why landslides initiate during earthquakes is important for both immediate and long term hazard mitigation, but can be difficult due to limitations of observational ground shaking data. In this study, we focus on the April 2015 M_w7.8 Gorkha earthquake, which caused 25,000 landslides in Nepal. Strong ground motion data are not available in the regions of high density landsliding from this event, making it impossible to directly relate ground shaking and landslide distribution. To circumvent this limitation, we model the ground shaking and topographic amplification from the Gorkha earthquake to better understand the distribution of coseismic landslides.

KEY FINDINGS

1. Topography, peak ground acceleration, and rock strength all play a role in the large scale coseismic landslide distribution.
2. The largest landslides initiated where the highest topographic amplification, highest elevations, and steepest slopes converged, typically in glacially sculpted terriain.
3. The source ridge of the largest and most devastating landslide in the Langtang Valley is unique within the modeled region having experienced three previously unknown episodes of strong amplification throughout the rupture due to the orientation of the ridge with respect to the propagating wavefield.

TECTONIC SUMMARY

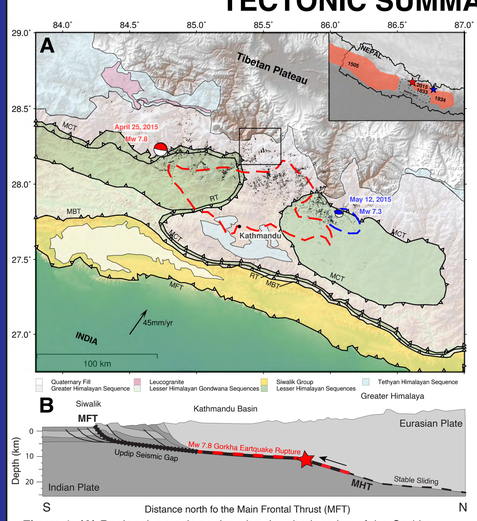

Figure 1: (A) Regional tectonic setting showing the location of the Gorkha mainshock (red moment tensor, moved to epicenter) and largest aftershock (Mw 7.3, blue moment tensor, moved to epicenter). Red and blue dashed lines show 2m slip contours of each rupture. Black polygons are locations of landslides from Roback et al., 2018[4]. Geologic map from DeCelles et al., 2020 overlays the topography with units labeled in the legend below[5]. Langtang Valley is highlighted in the black box. Inset shows location of mainshock (red star) and aftershock (blue star) in the context of Nepal. Red regions are major paleo-ruptures - 1505 ~Mw 8.2-8.9,1934 ~Mw 8.4, 1833 ~Mw 7.8 with an indistinguishable rupture area from the 2015 earthquake[6]. Possible seismic gap is denoted in the black dashed polygon.**(B)** Cross section showing the Main Himalaya Thrust (MHT) and the 2015 epicenter at depth (red star) modified from Bilham, 2019[8]. The red dashed line approximates the location of the rupture along the MHT. The thick dashed line represents the updip seismic gap and the thin dashed line represents the region of stable sliding along the detachment at depth. MHT – Main Himalaya Thrust, MCT – Main Central Thrust, MBT – Main Boundary Thrust, MFT – Main Frontal Thrust, RT – Ramgarth Thrust

When: April 25, 2015
Where: Nepal, ~80km NW of the capital city of Kathmandu (population ~1mil), 12km-depth, unzipped the lower portion of the Main Himalaya Thrust[1] (MHT) (Fig1 A,B)
Magnitude: Mw 7.8
Devastation: *Fatalities* - 9,000 *Injuries* - 23,000, *Damage* – $1 billion USD[2]
Rupture: ~150km to the east of the epicenter, did not break the surface
Aftershocks: ~600 events 45 days after the mainshock, the largest a Mw7.2 on May 12, 2015[3]
Coseismic Landslides: 25,000 (black polygons Fig 1), database from Roback et al., 2018[4], many likely caused by topographic amplification (Fig 2)

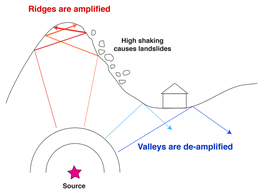

Figure 2: Schematic of topographic amplification. Ridge is amplified through focusing of seismic waves and valley is de-amplified through scattering of waves away from the free surface.

RESULTS

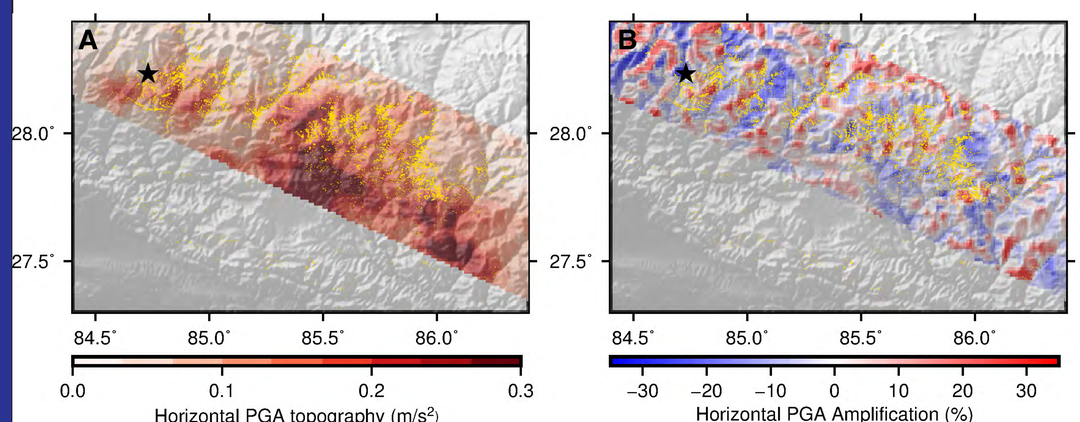

Figure 5: PGA and topographic amplification are calculated for a swath of synthetic seismometers filtered to 0.67Hz and with 1000m spacing. **(A)** Horizontal PGA of the high resolution topography mesh. **(B)** Amplification of Horizontal PGA calculated by taking the percent difference between simulations with high resolution and smoothed topography. Yellow polygons represent the full landslide area from Roback et al., 2018. The black star is the epicenter of the Gorkha earthquake and topography is 500m resolution, the same as the high resolution mesh.

LARGE SCALE LANDSLIDE TRENDS

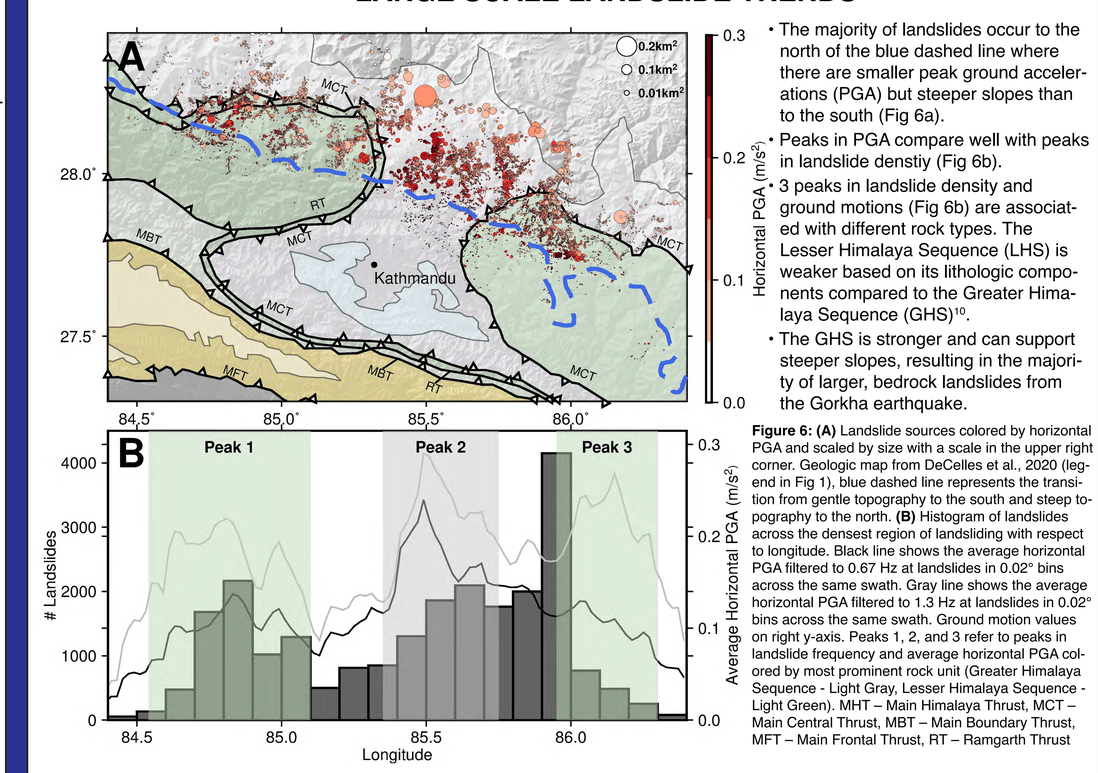

- The majority of landslides occur to the north of the blue dashed line where there are smaller peak ground accelerations (PGA) but steeper slopes than to the south (Fig 6a).
- Peaks in PGA compare well with peaks in landslide denstiy (Fig 6b).
- 3 peaks in landslide density and ground motions (Fig 6b) are associated with different rock types. The Lesser Himalaya Sequence (LHS) is weaker based on its lithologic components compared to the Greater Himalaya Sequence (GHS)[10].
- The GHS is stronger and can support steeper slopes, resulting in the majority of larger, bedrock landslides from the Gorkha earthquake.

Figure 6: (A) Landslide sources colored by horizontal PGA and scaled by size with a scale in the upper right corner. Geologic map from DeCelles et al., 2020 (legend in Fig 1), blue dashed line represents the transition from gentle topography to the south and steep topography to the north. **(B)** Histogram of landslides across the densest region of landsliding with respect to longitude. Black line shows the average horizontal PGA filtered to 0.67 Hz at landslides in 0.02° bins across the same swath. Gray line shows the average horizontal PGA filtered to 1.3 Hz at landslides in 0.02° bins across the same swath. Ground motion values on right y-axis. Peaks 1, 2, and 3 refer to peaks in landslide frequency and average horizontal PGA colored by most prominent rock unit (Greater Himalaya Sequence - Light Gray, Lesser Himalaya Sequence - Light Green). MHT – Main Himalaya Thrust, MCT – Main Central Thrust, MBT – Main Boundary Thrust, MFT – Main Frontal Thrust, RT – Ramgarth Thrust

LANGTANG VALLEY LANDSLIDE

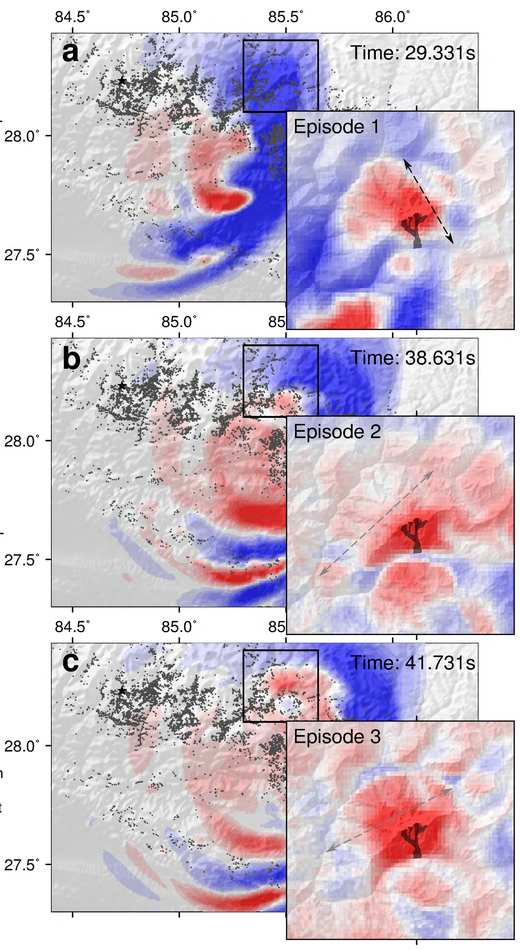

Figure 8: Episodes of the topographic amplification of the source ridge of the Langtang Valley landslide (a-c) Snapshots of the north component of the velocity wavefield at times where the Langtang ridge is amplified due to topography, red and blue are north (+) and south (-) velocity, respectively, colors saturated between -10cm/s and 10cm/s. Insets show a zoom in of the three episodes of amplification at the Langtang ridge colored by velocity amplification, here, the difference between the topography and smoothed simulations. Red and blue are positive and negative amplification, respectively, colors saturated between -3cm/s and 3cm/s. The five regions of initiation of the landslide from Lacroix, 2016 are shown in the inset as black polygons. The dashed arrows designate the approximate direction of shear particle motion that amplified the wavefield during that episode. Black denontes polarization along the minor ridge axis and gray denotes polarization along the major ridge axis.

The Langtang Valley landslide was the largest and most devastating landslide caused by the shaking from the Gorkha earthquake. This debris avalanche initiated in a glacier positioned at > 7 km elevation, mobilizing ice, snow, and rock that continued downslope until ~4.5 km elevation where it became airborne and descended into the river valley below[13,14]. The large volume of debris (estimated to have an accumulated volume of 6.95 x 106 m^3)[15] and an air blast from the landslide destroyed the village in the Langtang Valley below, killing ~350 people[14].

Snapshots of the wavefield and topographic amplification (Fig 8a-c) show that the source ridge of the Langtang Valley landslide was amplified 3 different times throughout the rupture (Fig 8a-c insets). This is due to the orientation of the ridge relative to the propagating wavefield and no other ridge with the high susceptibility of this ridge (slope, orientation, hillslope length) experienced multiple episodes of amplification. Episodes of amplification show shear motion either polarized perpendicular or parallel to the major ridge axis. The 5 points of initiation mapped by Lacroix, 2016 overlap with the episodes of amplification, **leading us to conclude that the Langtang valley landslide was likely caused by dynamic topographic amplification of the source ridge.**

METHODS

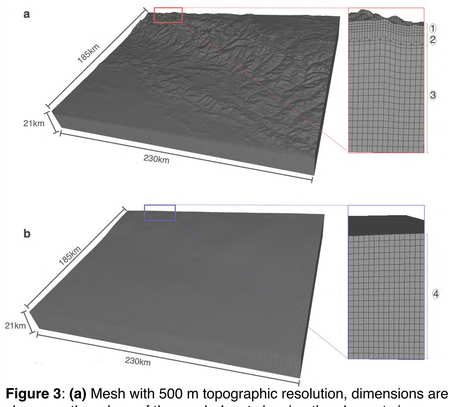

Figure 3: **(a)** Mesh with 500 m topographic resolution, dimensions are shown on the edges of the mesh. Inset showing the element sizes and the doubling layer. (1) is a 2 km thick layer with 500 m elements, (2) is the doubling layer, (3) is the 19 km thick layer with 1000 m elements. **(b)** Mesh with 20 km spatially averaged topography (smoothed mesh) with the same dimensions as the mesh in (a). Inset shows the constant element size of 1000m. (4) is the 21km thick layer with 1000 m elements.

We use the Spectral Element Method (SEM)[7] implemented in SPECFEM3D[8] to simulate ground motions in both a 500m resolution topography mesh (Fig 3a) and a smoothed topography mesh (Fig 3b), the comparison of which gives us a value of topographic amplification. The meshes are contructed using the SPECFEM3D internal mesher with a bulk element size of 1km and homogeneous elastic parameters, giving us a maximum resolved frequency of ~1.4Hz.We use the kinematic source model from Wei et al., 2018 (Fig 4)[9]. We interpolate the subfaults from 8 x 8 km to 1 x 1 km to appropriately sample the source at the resolution of the mesh.

Figure 4: Slip model from Wei et al., 2018 discretized into 1 x 1 km subfaults and colored by slip. Red star denotes the epicenter of the rupture, black arrow showing the direction of the rupture to the SE. Black square is showing the extent of the mesh from Fig 3. Kathmandu and Gorkha locations are labeled.

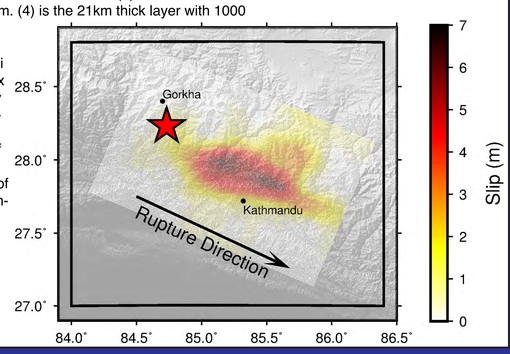

TOPOGRAPHIC AMPLIFICATION AND LANDSLIDE INITIATION

By taking the topographic amplification value at each landslide source location, we can evaluate the effect of topography on landslide initiation. Fig 7a shows landslides in regions experiencing topographic amplification and Fig 7b shows landslides experiencing topographic de-amplification. Landslides that are amplified are on average 40% larger than landslides that are de-amplified, showing the control topographic amplification has on landslide size. We also see that amplified landslides are distributed throughout the hillslope whereas de-amplified landslides are focused at the base of the hillslope, where there is potentially heightened landslide susceptibility (histogram insets).

The largest landslides typically initiate in regions that are amplified at high elevations and with steep slopes (Fig 7c). These landslides are also associated with glacially sculpted terrain, which is characterized by steeper, longer hillslopes and can produce deeper-seated landslides than more highly vegetated slopes at lower elevations[4,11]. As glaciers continue to thin and retreat at increasing rates in the Himalaya due to climate change, the topography that is left behind is primed for increased topographic amplification that could produce larger and more devastating coseismic landslides from future earthquakes.

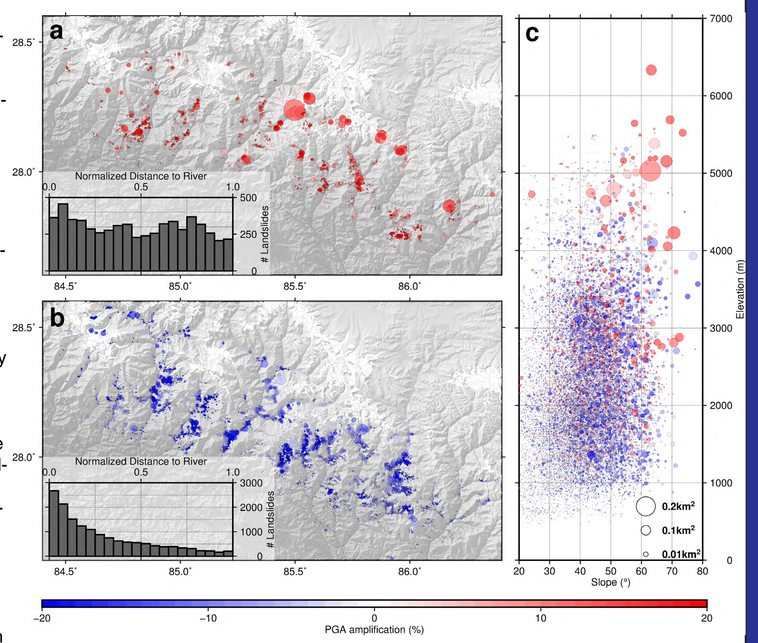

Figure 7: **(a)** Landslides in positive regions of amplification. Inset shows histogram of the distribution of positively amplified landslides with respect to the normalized distance to the closest river (0 is at a river and 1 is at a ridge). **(b)** Landslides in negative regions of amplification. Inset shows histogram of the distribution of negatively amplified landslides with respect to the normalized distance to the closest river (0 is at a river and 1 is at a ridge). Distance to river is normalized by dividing the river distance by the combined ridge and river distance (i.e. slope length). White polygons are mapped glaciers since 2008 from the GLIMS database[12]. **(c)** Scatter plot of elevation vs. slope of landslide sources coloured by amplification and scaled by landslide source surface area. Legend for circle size of all plots in c.

CONCLUSIONS AND FUTURE WORK

- Wavefield simulations from this study reveal that by taking into account topography, rupture properties, and glaciated or deglaciated terrain, we may be able to more effectively estimate where the highest concentration of landslides and the largest landslides are most likely to occur during an earthquake.
- Our modeling approach may be applied in regions of high seismic potential to evaluate the coseismic landslide hazard for potential rupture scenarios.
- We plan to apply this modeling to potential earthquakes in the central Himalayan seismic gap (Fig 1) to better understand how topographic amplification, and therefore the potential of large landslides, could effect the region during a large, future, earthquake.
- We also plan to investigate the effect of ice cover on topographic amplification using simple models as well as large scale examples to understand its role in large ground failures.

REFERENCES

1. Avouac, J.-P., Meng, L., Wei, S., Wang, T. & Ampuero, J. P. Lower edge of locked Main Himalayan Thrust unzipped by the 2015 Gorkha earthquake. Nat. Geosci. 8, 708–711 (2015).
2. Zhao, B. April 2015 Nepal earthquake: observations and reflections. Nat. Hazards 80, 1405–1410 (2016).
3. Adhikari, L. B. et al. The aftershock sequence of the 2015 april 25 Gorkha-Nepal earthquake. Geophys. J. Int. 203, 2119–2124 (2015).
4. Roback, K. et al. The size, distribution, and mobility of landslides caused by the 2015 Mw 7.8 Gorkha earthquake, Nepal. Geomorphology 301, 121–138 (2018).
5. DeCelles, P. G., Carrapa, B., Ojha, T. P., Gehrels, G. E. & Collins, D. Structural and Thermal Evolution of the Himalayan Thrust Belt in Midwestern Nepal. Geol. Soc. Am. Spec. Pap. 547, 1–78 (2020).
6. Bilham, R. Himalayan earthquakes: a review of historical seismicity and early 21st century slip potential. Geol. Soc. London, Spec. Publ. 483, 423–482 (2019).
7. Patera, A. T. A spectral element method for fluid dynamics: Laminar flow in a channel expansion. J. Comput. Phys. 54, 468–488 (1984).
8. Komatitsch, D. & Tromp, J. Introduction to the spectral element method for three-dimensional seismic wave propagation. Geophys. J. Int. 139, 806–822 (1999).
9. Wei, S. et al. The 2015 Gorkha (Nepal) earthquake sequence: I. Source modeling and deterministic 3D ground shaking. Tectonophysics 722, 447–461 (2018).
10. Cannon, J. M., Murphy, M. A. & Taylor, M. Segmented strain accumulation in the High Himalaya expressed in river channel steepness. Geosphere 14, 1131–1149 (2018).
11. McColl, S. T., Davies, T. R. H. & McSaveney, M. J. The effect of glaciation on the intensity of seismic ground motion. Earth Surf. Process. Landforms 37, 1290–1301 (2012).
12. Raup, B. et al. The GLIMS geospatial glacier database: A new tool for studying glacier change. Glob. Planet. Change 56, 101–110 (2007).
13. Collins, B. D. & Jibson, R. W. Assessment of existing and potential landslide hazards resulting from the April 25, 2015 Gorkha, Nepal earthquake sequence. Open-File Report (2015). doi:10.3133/ofr20151142
14. Kargel, J. S. et al. Geomorphic and geologic controls of geohazards induced by Nepal's 2015 Gorkha earthquake. Science 351, 1–18 (2016).
15. Lacroix, P. Landslides triggered by the Gorkha earthquake in the Langtang valley, volumes and initiation processes. Earth, Planets Sp. 68, 1–10 (2016).